16th World Conference on Earthquake Engineering, 16WCEE 2017

Santiago Chile, January 9th to 13th 2017

Paper N° 3542

Registration Code: S-R145929985

FATIGUE BEHAVIOR OF STEEL SLIT-DAMPERS WITH VARIOUS SHAPES

Y. Jiao[1], M. Saito[2], M. Kohno[3]

[1] *Assistant Professor, Tokyo University of Science, yujiao@rs.tus.ac.jp*
[2] *Student, Tokyo University of Science, mami.mnop24@gmail.com*
[3] *Professor, Tokyo University of Science, kohno@rs.kagu.tus.ac.jp*

Abstract

Passive control structural systems with seismic dampers have achieved significant progress in recent decades. In this structural system, dampers dissipate most of the earthquake-induced energy to minimize damage to the parent structure. Steel slit-dampers, which are known to have stable and large energy dissipation capacity, are a type of such hysteretic dampers. This kind of dampers is fabricated by simply cutting slits on steel plates, leaving a number of strips in between. All slits are rounded at their ends to reduce stress concentration. High tension bolts are set at the end of the plates to connect the dampers to the parent structures. Each strip behaves as a fixed-ended beam and deforms in double curvature, while plastic hinges form at the end of the strips to dissipate energy under deformation. Slit-dampers are light-weight and can be easily set and replaced at various locations in the structures where necessary. By changing the shape of the damper, its stiffness and strength can be adjusted to different levels to meet the needs of structural design. Research has been done related to slit-dampers' low cycle fatigue behavior and hysteretic characteristics. Cyclic loading tests were performed, which demonstrated the dampers' stable hysteretic behavior and adequate energy dissipation capacity. Nevertheless, in most of the current research work, only slit-dampers with very limited geometries were studied, while "shape" is one of the most important variables in the design of the structures with slit-dampers, which would strongly affect the fatigue behavior/plastic deformation capacity of the dampers. In order to achieve desired structural performance, slit-dampers with suitable sizes for a structure should be chosen considering the structure response under various types of earthquakes. A practical design guideline for structures with slit-dampers is necessary. However, there is no such design guideline at this moment to facilitate the implementation of this device. For the purpose of establishing a design guideline for slit-dampers, it is necessary to clarify how geometric shapes affect the fatigue behaviour of slit-dampers. In this paper, experimental study of slit-dampers with various shapes was carried out. Basic information of the influence of geometries on the behavior of slit-dampers is obtained from the tests. However, it is impossible to cover all the shape parameters in the experiments. Therefore, based on the previous experimental study, FEM analyses of slit-dampers with various shapes were also conducted. The equivalent strain amplitude at the fracture zone (toe of the strip where the ductile cracks start) is studied through the analytical results. For dampers with different shapes, the relationship between the equivalent strain amplitude and the number of loading cycles until the ultimate state of a slit-damper was found following the Manson-Coffin law. The influence of geometry on the fatigue behaviour & energy dissipation capacity of steel slit-dampers was evaluated based on the experimental and analytical results.

Keywords: steel slit-damper, low cycle fatigue, cyclic loading test, FEM analysis, equivalent strain amplitude

1. Introduction

Passive control structural systems with seismic dampers have achieved significant progress in recent decades (for example: [1][2]). In this type structural system, dampers dissipate most of the earthquake-induced energy, which makes it possible to minimize damage to the parent structures [3]. The energy dissipation of dampers can be achieved through different mechanisms: friction, plastification of metals, deformation of viscoelastic solid or liquid, etc. In particular, one of the most popular dampers is the hysteretic dampers usually made of metallic materials. Generally, during moderately severe earthquakes these dampers act as stiff members which reduce structural deformations, while during very severe earthquakes hysteretic dampers dissipate the earthquake input energy [4].

There are many kinds of hysteretic dampers such as steel triangular plate dampers TADAS [5], buckling restrained braces (for example: [6]), honeycomb dampers [7] and steel slit-dampers [8]. Among them, steel slit-dampers are known to have stable and large energy dissipation capacity. This kind of dampers is fabricated by simply cutting slits on steel plates, leaving a number of strips in between (Fig. 1). All slits are rounded at their ends to reduce stress concentration. High tension bolts are set at the end of the plates to connect the dampers to the parent structures. Each strip behaves as a fixed-ended beam and deform in double curvature. Plastic hinges form at the end of the strips to dissipate energy under deformation. This kind of device is light-weight and can be easily set and replaced at various locations in the structures where necessary. By changing the shape of the damper, its stiffness, strength, and energy dissipation capacity can be adjusted to different levels to meet the needs of structural design. Moreover, steel slit-dampers are sensitive to small deformation too. Therefore, they are not only effective under large deformation due to major earthquakes. Under long duration earthquake with relatively small deformation amplitude, slit-dampers are also helpful in restraining structural shaking.

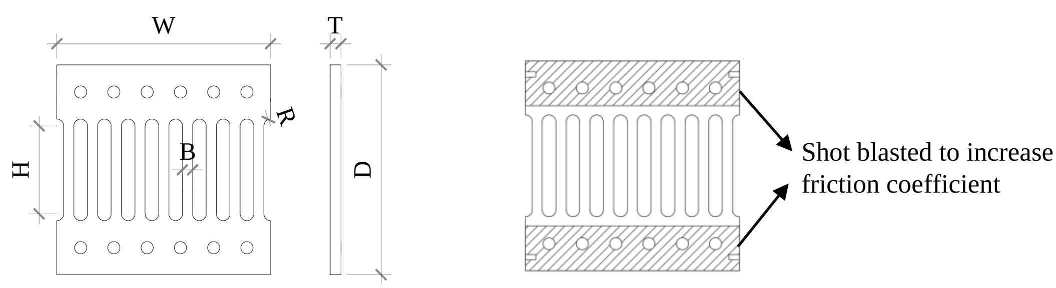

Fig. 1 Shape parameters of slit-damper specimens

Research has been done related to the low cycle fatigue behavior and hysteretic characteristics of dampers. Cyclic loading tests were performed; the results demonstrated stable hysteretic behavior and adequate energy dissipation capacity [9]. In [8] real time speed tests were carried out, the results indicated that loading speed does not seem to affect the damper’s hysteretic characteristics significantly. However, in most of the current research work, only slit-dampers with very limited geometries were studied, while “shape” is one of the most important variables in the design of slit-dampers as well as the structures with slit-dampers inside. As a result, there is no practical design guideline for structures with slit-dampers which makes it difficult to use this type of device. To establish a design guideline for slit-dampers, it is necessary to clarify how geometric shapes affect the fatigue behaviour of slit-dampers.

In [10], the authors performed a preliminary experimental study of slit-dampers of various shapes. Some basic information about the influence of geometries on the behavior of slit-dampers was obtained through experiments. The dampers’ energy dissipation capacity and fatigue life were studied. It was indicated that the local strain history at the toes of the strips has a strong relationship with the low cyclic fatigue behavior of the damper. In the present paper, more experiments were carried out to enrich the variables. Moreover, since it is impossible to cover all the shape parameters in the experiments. Therefore, FEM analyses of slit-dampers with various shapes were also conducted using the experimental results as calibration. The equivalent strain amplitude at the fracture zone (toe of the strip where the ductile cracks start) is studied through the analytical results. For dampers with different shapes, the relationship between the equivalent strain amplitude and the number of loading cycles until the ultimate state of a slit-damper was found following the Manson-Coffin law. The influence of geometry on the fatigue behavior & energy dissipation capacity of steel slit-dampers was evaluated based on the experimental and analytical results.

2. Cyclic loading tests of steel slit-dampers

2.1 Basic information of the specimens

Seven types of slit-dampers specimens were tested under cyclic loading histories with constant deformation amplitudes. For each specimen type, 3 specimens were prepared for the tests under loading histories with different deformation amplitudes. Same as in the work of reference [10], all specimens in this experiment were flexural yielding members where bending moment is the main reason that causes yielding of the dampers. The main parameters in this study include: radius at the end of the slits (R), depth of the strips (B), number of the strips (N), thickness of the damper plate (T), and length of parallel sections of the strips (H). Fig. 1 and Table 1 show the basic information of the specimens, together with the information of the specimens tested in [10]. Specimens SLD_1~SLD_4 were described in [10]. Specimen SLD_1 was regarded as the basic model in these tests, other specimens were designed by changing one or more shape parameters, shadowed in grey. Among them, specimens SLD_5 had a lower height; specimens SLD_6~SLD_10 were 4mm thicker than specimen SLD_1 with H, B, and R varing as well; and SLD_11 was 25mm thick.

Blast furnace steel plate (SN400B) is used to make the specimens. SN400B steel [11] is one of the structural steel that is commonly used in Japan in recent years in steel buildings. Fig. 2 shows the stress-strain relationship of the material (T=16mm) obtained from coupon tests using JIS-1A test pieces [12]. The yield strength, ultimate strength, and elongation are listed in Table 2.

Table 1 Geometries of all specimens

No.	Name	D (mm)	W (mm)	T (mm)	H (mm)	B (mm)	R (mm)	N
SLD_1 [10]	D310T16B15R10	310	315	16	130	15	10	9
SLD_2 [10]	D310T16B15R15	310	405	16	120	15	15	9
SLD_3 [10]	D310T16B20R10	310	360	16	130	20	10	9
SLD_4 [10]	D310T16B15R10N13	310	455	16	130	15	10	13
SLD_5	D250T16B15R15	250	315	16	70	15	10	9
SLD_6	D310T22B15R10-a	310	315	22	130	15	10	9
SLD_7	D310T22B15R5	310	225	22	140	15	5	9
SLD_8	D310T22B15R10-b	310	315	22	130	15	10	9
SLD_9	D310T22B20R10	310	360	22	130	20	10	9
SLD_10	D310T22B15R15	310	360	22	130	15	15	9
SLD_11	D310T25B15R10	310	315	25	130	15	10	9

Table 2 Mechanical characteristics of the materials

Material	Yield strength (N/mm^2)	Ultimate strength (N/mm^2)	Elongation (%)
T16-SLD_1~5	300	433	36
T22-SLD_6	240	395	36
T22-SLD_7~10	278	414	33
T25-SLD_11	249	404	35

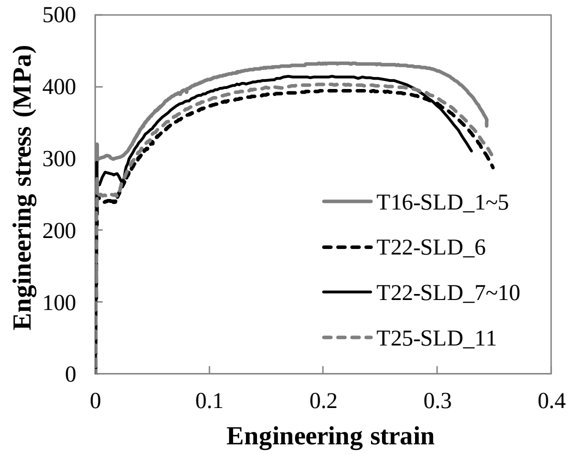

Fig. 2 Stress-strain relationship of the materials from coupon tests

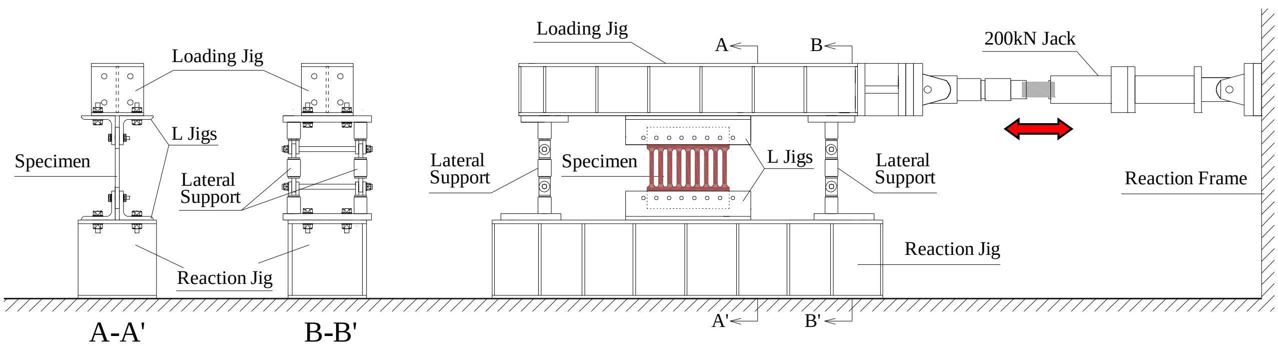

Fig. 3 Experiment setup

2.2 Test setup and loading programs

Fig. 3 shows the test setup details. The specimen was connected to L shape jigs at top and bottom parts through M16 high tension bolts to form the fixed connections. The lower L shape jigs were set up through the reaction jig, with the latter fastened onto the reaction frame to offer horizontal and vertical support. A loading jig connecting the upper L shape jigs and the oil jack (maximum load capacity of 200kN) which was installed horizontally on the reaction frame composed the loading system. Moreover, lateral supports (stiffening systems) consisting of 4 truss members were set at both sides of the specimen to avoid out-of-plane deformation of the whole system. At the same time, this stiffening system was capable to deform following the trail of the specimen under horizontal loading, in other words, to keep the loading jig horizontal during the tests. The loading direction is shown in Fig. 3. Loading history is another variable of the experiment. For each type of damper specimen (three specimens), three deformation-controlled cyclic loading histories with different constant amplitudes were employed. The amplitudes are listed in Table 3.

2.3 Measuring system

Four displacement transducers (LVDT) were set up to measure the shear deformation (δ) of the specimens, which is defined in Eq. (1). Locations of these transducers are shown in Fig. 4a. Shear force is recorded through the built-in load cell in the oil jack. Notice that in order to obtain the horizontal force applied to the damper; one displacement transducer (LVDT) was set to record the rotation of oil jack's loading end. Fig. 4b shows the strain gauge arrangements. High-yield strain gauges, which work effectively under large strain, were attached to the ends of the parallel sections in both sides and the middle strips where significant strain concentration is expected to occur. Elastic strain gauges were attached at the center of the above mentioned strips (front and back sides) to track the axial force in the specimen.

$$\delta = \frac{(|\delta_1| + |\delta_2|) - (|\delta_3| + |\delta_4|)}{2} \tag{1}$$

where δ_1 and δ_2 are the deformation recorded at the top (left & right) of the damper specimens; δ_3 and δ_4 are the deformation recorded at the bottom (left & right) of the specimens.

3. Experimental results

3.1 Ultimate states and load-deformation relationships

Each specimen was loaded until fracture during the tests. Ductile cracks initiated at the toe of each strip close to the rounded toes of the slits during the loading of all specimens. Under further loading, those cracks propagated wider and longer, which led to the decrease of the load carrying capacity of the dampers. Fig. 5 shows the failure of specimen SLD_6 and its ductile cracks as an example. The ultimate states of the slit-dampers were defined to be the point when the maximum force of a certain cycle dropped below 90% of the maximum value, because the maximum force of each cycle decreased rapidly after it dropped below 90% of the maximum value during the whole loading procedure, as mentioned in [10]. The number of loading cycles until the ultimate states of each specimen is listed in Table 3.

The force-rotation relationships from SLD_6 and SLD_11 are shown in Fig. 6 as examples, with the 90% maximum force points noted with red marks. For each type of specimen, the experimental results under 3 different loading histories are shown. These graphs indicate stable hysteresis loops of all specimens until the ultimate states of the dampers, which could be simplified as bi-linear hysteretic models. The yield point and maximum force of SLD_11 are larger than those of SLD_6 due to larger thickness of the steel plate.

3.2 Strain states

To each specimen, 6 high-yield strain gauges were attached to the end of the strips. As an example, the strain histories (first three cycles) at the end of one of the strips' parallel sections from SLD_10 are shown in Fig. 7. Under the rotation amplitude of 0.27rad, the strain recorded in the first loading cycle reached 10%, which damaged the strain gauge. Therefore, only the data under the amplitude of 0.107 and 0.053 are shown. The strain under larger loading amplitude grew significantly during the tests, which also showed rapid increase in each cycle. Although the strain histories shifted slightly to the tension side during loading due to the residual strain after plastification, the strain amplitude in each loading cycle is similar to each other.

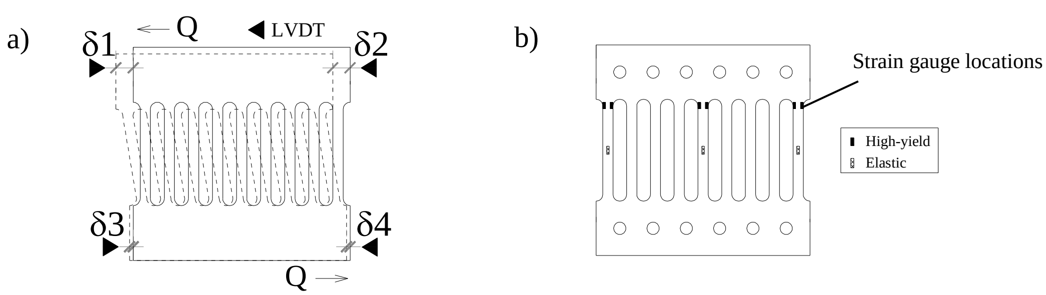

Fig. 4 Measuring system

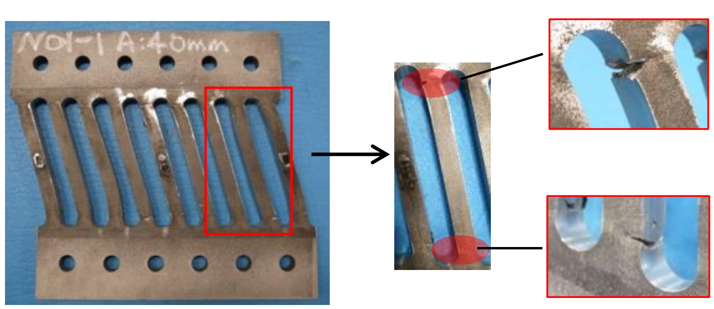

Fig. 5 Specimen SLD_6 after loading (ductile cracks at the toe of the strip)

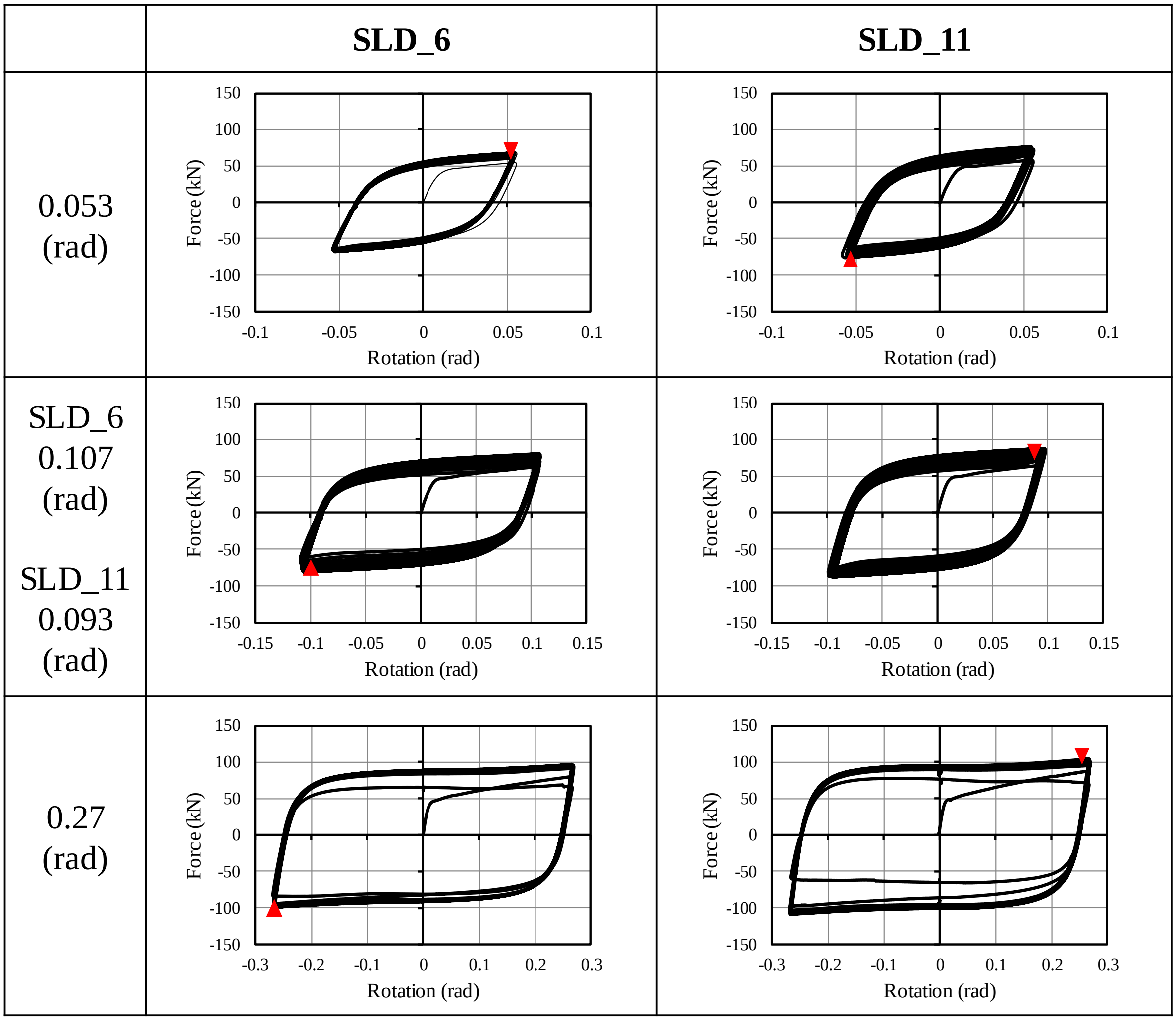

Fig. 6 Force-rotation relationships of SLD_6 and SLD_11

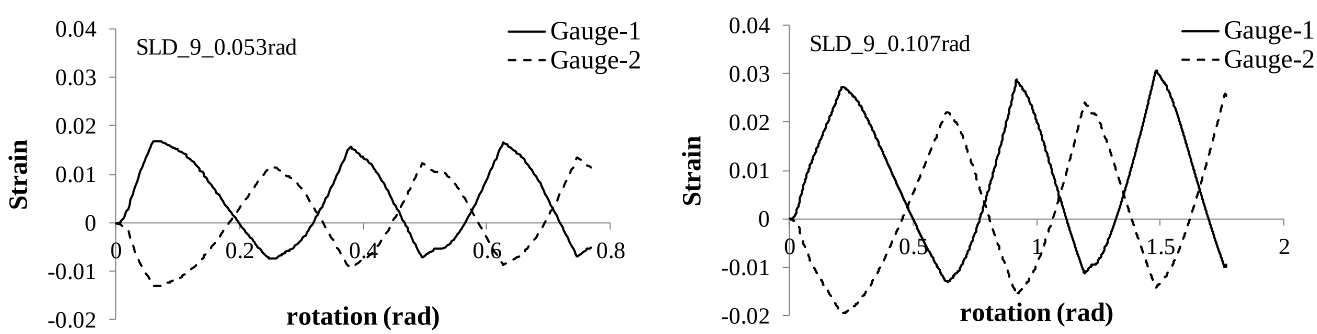

Fig. 7 Strain histories of SLD_9 (0.053rad & 0.107rad)

3.3 Low cyclic fatigue behavior

The fatigue behavior (Manson-Coffin relations [13][14]) of all specimens are plotted in the log-log graph (Fig. 8). The X-axis is the full amplitude of each loading history, and the Y-axis is the number of loading cycles to the ultimate state. The number of loading cycles decreases while the deformation amplitude increases. For each type of specimens, linear relations can be found between the plots. However, for the specimens of different geometries and materials, different Manson-Coffin relations are observed. It is difficult to obtain an universal evaluation method of the fatigue life of slit-dampers with different through experiments only. In the next section, FEM analysis method is introduced to discuss the influence of damper shape to its fatigue behavior.

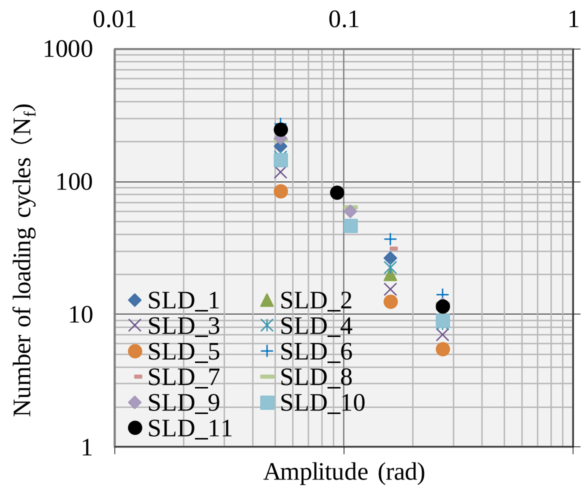

Fig. 8 Fatigue behavior of the specimens

Table 3 Fatigue life & equivalent strain amplitude of the specimens

No.	SLD_1 [10]			SLD_2 [10]			SLD_3 [10]		
Amplitude (rad)	0.27	0.16	0.053	0.27	0.16	0.053	0.27	0.16	0.053
N_f	11	26.5	184.5	10	20	147.5	7	15.5	118.5
ε_{eq}	0.26	0.166	0.059	0.278	0.18	0.065	0.329	0.211	0.077
No.	SLD_4 [10]			SLD_5			SLD_6		
Amplitude (rad)	0.27	0.16	0.053	0.27	0.16	0.053	0.27	0.16	0.053
N_f	8.5	22.5	153.5	5.5	12.5	85.5	14	37	272
ε_{eq}	0.26	0.166	0.059	0.35	0.224	0.08	0.244	0.162	0.059
No.	SLD_7			SLD_8			SLD_9		
Amplitude (rad)	0.27	0.16	0.053	0.27	0.107	0.053	0.27	0.107	0.053
N_f	12	31.5	152	12	64	206.5	12	60	212
ε_{eq}	0.217	0.144	0.055	0.248	0.111	0.057	0.242	0.114	0.059
No.	SLD_10			SLD_11					
Amplitude (rad)	0.27	0.107	0.053	0.27	0.093	0.053			
N_f	9	46.5	146	11.5	83.5	249			
ε_{eq}	0.314	0.14	0.072	0.267	0.106	0.062			

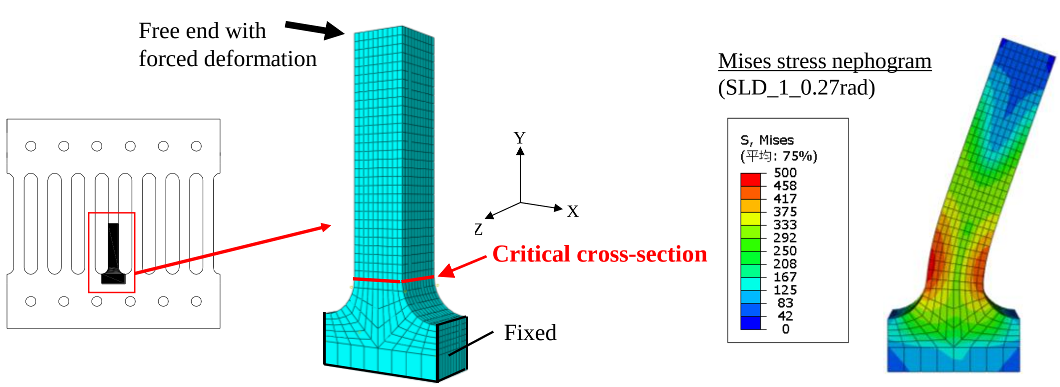

Fig. 9 FEM analytical model & the stress nephogram of SLD_1_0.27rad

4. FEM analyses of steel slit-dampers

4.1 Analytical model

As pointed out in [10], the fatigue behavior of slit-damper has a strong correlation with the local strain histories at the toe of each strip. From Fig.7 and [10], one can conclude that under cyclic loadings, the strain amplitude at the toe of the strip remains approximately constant in each cycle. Based on the above phenomenon, monotonic FEM analyses of steel slit-dampers were carried out. Attempts were made to establish an evaluation method of the damper's fatigue life through the local strain amplitudes.

Monotonic FEM analyses of the slit-damper specimens were conducted using Abaqus v6.14. Base on the symmetrical characteristics of slit-damper, analyses were performed to the lower half of a strip. The analytical model is shown in Fig. 9. Solid element (C3S8R) was employed in the analyses. The half strip is fixed on the bottom part, while on the top-end, deformation on Z-direction and rotation around X and Y-directions were restrained. Forced deformation was applied to the top-end via X-direction. The sizes of meshes in X and Y-directions were about 1.5mm to 2.25mm, and the mesh size in Z-direction (through-thickness direction) is no larger than 1.5mm.

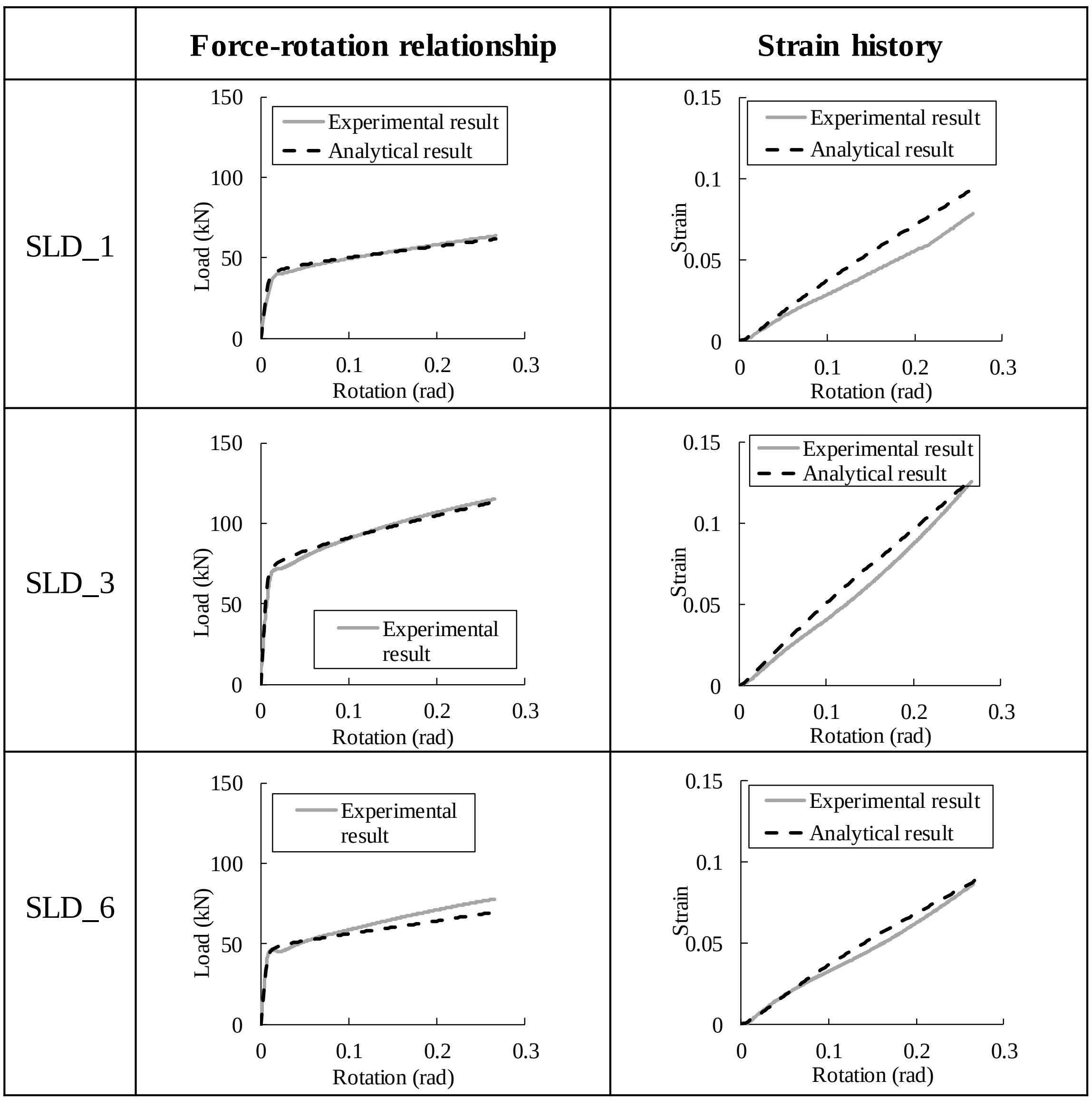

Fig. 10 Comparison of analytical and experimental results

For each specimen model, the corresponding material characteristics obtained through coupon tests were introduced. The Young's modulus was set to be 205GPa, and the Poisson coefficient was 0.3 as adopted in most of the analyses of steel elements. The von Mises stress was introduced to predict yielding of materials under any loading condition. In the analyses, geometric nonlinearity was taken into consideration.

4.2 Analytical results

As examples, Fig. 10 compares the force-deformation relationships of SLD_3, SLD_4, and SLD_6 obtained from the FEM analyses to the experimental results. The analytical output strain histories of these specimens at the location where the high-yield strain gauges were attached were also plotted in Fig. 10, together with the corresponding strain histories measured from the tests. From Fig. 10, one can find that the stiffness, yield strength and post-yield behavior from the analytical model match the experimental results quite well. Furthermore, the analytical strain histories also show good correspondences with the experimental results.

5. Fracture condition at critical cross-sections

5.1 Definition of critical cross-sections of the slit-damper

In the experiments, small ductile fractures initiated at the toe of the steel strip (the end of the straight section of the strip) of each specimen (Fig. 5). Those fractures propagated and elongated throughout the loading procedure that caused the decrease of force which led to the ultimate states. The stress nephogram of SLD_1 when the rotation is 0.27rad is shown in Fig. 9, which also indicates that the largest strain occurs right at the end of the straight section on the strip. Based on the above discussion, the critical cross-section (CCS) of the slit-damper is defined as the cross-section at the toe of each steel strip (Fig. 9).

5.2 Strain distribution at the critical cross-section from analyses

Fig. 11 illustrates the strain distributions along Z-direction (thickness) on both tension and compression edges of SLD_1 and SLD_6 at the CCS when the rotation is 0.27rad. The results show that the strain is not evenly distributed along the thickness direction due to complex triaxial stress states. Therefore, the mean strain through the thickness direction of each strip is calculated as the "strain at CCS".

The strain distribution on Z-direction (width) of the strip might be affected by the size of the radius at the end of the slits (R), considering stress concentration. A series of analysis was conducted using SLD_1 as the basic model, with R varying from 0mm, 5mm, 10mm, to 15mm. The strain distributions along width direction of the strips with different R are plotted in Fig. 12 (0.27rad). These graphs show that when R is larger than 5mm, the effect of stress concentration is negligible. The critical cross-section remains effectively plane even when the rotation is large. However, when R is less than 5mm, the plane section assumption is less valid. Steel slit-dampers with such small R are difficult to manufacture and obviously not a good choice for structural engineers.

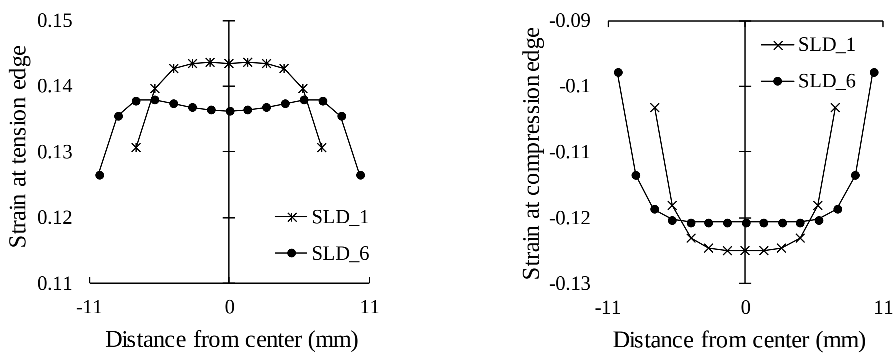

Fig. 11 Strain distributions along Z-direction

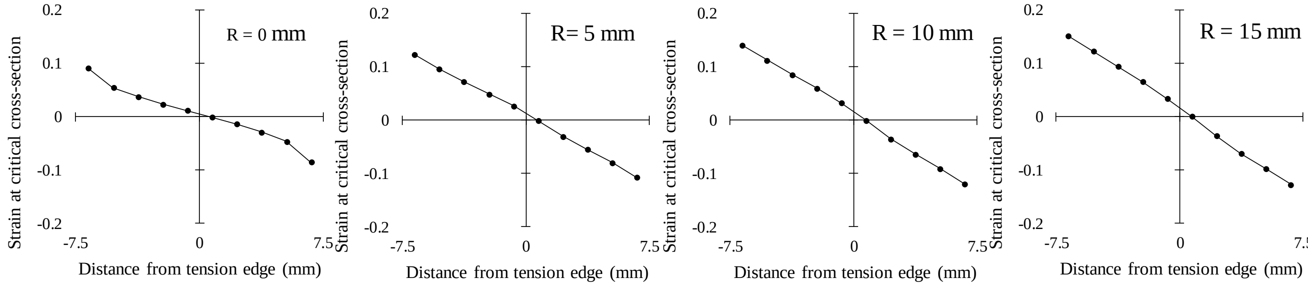

Fig. 12 Strain distributions along X-direction

In Fig. 12, strain at the tension and compression sides are not symmetric to each other, which is the result of geometry nonlinearity. Therefore, to evaluate the strain at CCS, it's necessary to take into consideration both the tension and compression strain. In the previous mentioned experiments, the strain amplitude of each loading cycle measured by the strain gauges almost remain constant (Fig. 5). Based on the above facts, the equivalent strain amplitude at CCS $\varepsilon_{\mathrm{eq}}$ is defined using Eq. (2).

$$\varepsilon_{\mathrm{eq}} = |\varepsilon_t| + |\varepsilon_c| \tag{2}$$

Here, ε_t and ε_c are the analytical strain value on the tension and compression edge, at CCS.

5.3 Fracture condition at the critical cross-section

Fatigue behavior of steel slit-dampers with different shape parameters is evaluated based on the equivalent strain amplitude at CCS $\varepsilon_{\mathrm{eq}}$. Fig. 13 shows the fracture condition at CCS. The numbers of loading cycles until the ultimate states of all specimens N_f, which are recorded in the experiment, are plotted on X-axis. While the corresponding $\varepsilon_{\mathrm{eq}}$ of each specimens obtained through monotonic FEM analyses are plotted on Y-axis. From the graph, one would notice that despite the different shape and material characteristics, the relationship between N_f and $\varepsilon_{\mathrm{eq}}$ follows the Manson-Coffin law. The Manson-Coffin relationship is expressed in Eq. (3):

$$\varepsilon_{\mathrm{eq}} = 0.85 \cdot N_f^{\;-0.51} \qquad (0.054 \le \varepsilon_{\mathrm{eq}} \le 0.349) \tag{3}$$

With Eq. (3), the fatigue life of slit-dampers with various shapes can be predicted as long as the equivalent strain amplitude at CCS $\varepsilon_{\mathrm{eq}}$ is obtained from analysis.

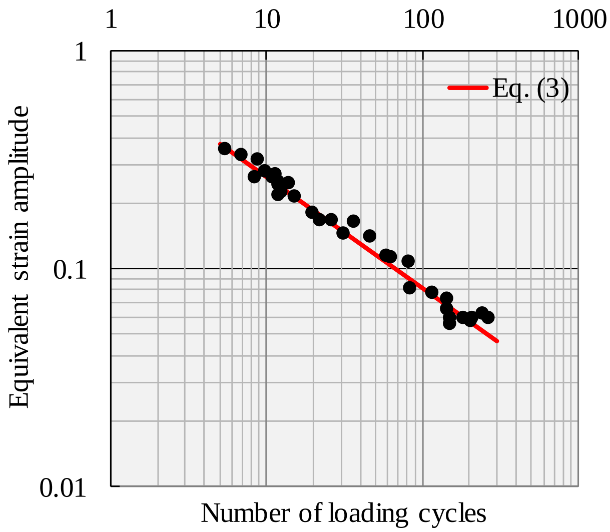

Fig. 13 Relationship between N_f and ε_{eq}

6. Conclusions

The present paper presents experimental and analytical study of steel slit-dampers with various shapes. The strain distribution at the toe of the steel strip (critical cross-section of slit-damper) is studied. The equivalent strain amplitude at CCS and the number of loading cycles until the ultimate state of a slit-damper is found to match very well to the Manson-Coffin relation. This relationship is not influenced by the shape of the damper. When the equivalent strain amplitude is obtained through analysis, it is possible to predict the fatigue life of steel slit-dampers using Eq. (3).

7. References

[1] Roeder, C.W., and Popov, E.P. (1977), "Inelastic Behavior of Eccentrically Braced Steel Frames Under Cyclic Loadings". Report No. UCB/EERC-77/18, Earthquake Engineering Research Center, College of Engineering, University of California Berkeley, Berkeley, CA.

[2] Uang, C.U, Nakashima, M., and Tsai K.C. (2004), "Research and Application of Buckling-Restrained Braced Frames," Steel Structures 4(2004) 301-313.

[3] Wada, A., Shimitsu, K., Kawaai, H., Iwata, M., and Abe, T. (1998), "Damage Control Design of Building," Maruzen Inc.

[4] Skinner R.I., Kelly J.M., and Keine A.J.(1975), "Hysteretic Dampers for Earthquake-resistant Structures," Earthquake Engineering and Structural Dynamics, Vol.3, pp. 287-296.

[5] Tsai K.C., Chen H.W., Hong C.P., and Su Y.F.(1993), "Design of Steel Triangular Plate Energy Absorbers for Seismic ‐ Resistant Construction," Earthquake Spectra, Vol. 9, No. 3, pp. 505-528

[6] Maeda Y., Nakata Y., Iwata M., and Wada A.(1998), "Fatigue Properties of Axial-yield Type Hysteresis Dampers (In Japanese)," Journal of Structural and Construction Engineering, AIJ, No503, pp. 109-115

[7] Kobori T., Miura Y., Fukusawa E., Yamada T., Arita T., Takenake Y., et al.(1992), "Development and Application of Hysteresis Steel Dampers," Proceedings of 11th World Conference on Earthquake Engineering. pp. 2341–6.

[8] Wada A., Huang Y.H., Yamada T., Ono Y., et al. (1997) "Actual Size and Real Time Speed Tests for Hysteretic Steel Damper," Proceedings of STESSA'97, pp. 778–785.

[9] Chan R.W.K., and Albermani F. (2008) "Experimental study of steel slit damper for passive energy dissipation," Engineering Structures, 30, pp. 1058–1066.

[10] Yu Jiao, Yukako Katsuyama, and Mamoru Kohno, Cyclic loading tests of steel slit-dampers with various shapes. 10th International Conference on Urban Earthquake Engineering (10CUEE), Tokyo, 2013.3.

[11] Rolled steels for building structure. Japanese Industrial Standards, JIS G 3136:2012

[12] Architectural Institute of Japan. Japanese architectural standard specification JASS 6, steel work (In Japanese). Tokyo: AIJ; 1996.

[13] Manson S.S.(1954), Behavior of materials under conditions of thermal stress, NASA TND, 2933

[14] Coffin L.F. JR., Schenectady N.Y. (1954), A study of the effect of cyclic thermal stresses on a ductile metal, Transactions of the ASME,pp.931-950

[15] von Mises, R. (1913). Mechanik der festen Körper im plastisch deformablen Zustand. Göttin. Nachr. Math. Phys., vol. 1, pp. 582–592.